

Classical simulation and theory of quantum annealing in a thermal environment

Hiroki Oshiyama,^{1,*} Sei Suzuki,^{2,†} and Naokazu Shibata^{1,‡}

¹*Department of Physics, Tohoku University, Sendai 980-8578, Japan*[§]

²*Department of Liberal Arts, Saitama Medical University, Moroyama, Saitama 350-0495, Japan*

We study quantum annealing in the quantum Ising model coupled to a thermal environment. When the speed of quantum annealing is sufficiently slow, the system evolves following the instantaneous thermal equilibrium. This quasistatic and isothermal evolution, however, fails near the end of annealing because the relaxation time grows infinitely, therefore yielding excess energy from the thermal equilibrium. We develop a phenomenological theory based on this picture and derive a scaling relation of the excess energy after annealing. The theoretical results are numerically confirmed using a novel non-Markovian method that we recently proposed based on a path-integral representation of the reduced density matrix and the infinite time evolving block decimation. In addition, we discuss the crossover between the adiabatic and quasistatic regimes and propose experiments on the D-Wave quantum annealer.

Introduction.—

The quantum annealing (QA) device manufactured by D-Wave Systems has made an immense impact not only in the physics community but also in the industrial community with a hope of developing quantum computers and simulators [1–9]. It is known that this device carries out QA imperfectly in the sense that the system embedded in this device is affected by its environment [1, 10, 11]. This fact raises issues regarding QA dynamics in a thermal environment [2, 12–18].

QA was proposed as a quantum mechanical algorithm to solve combinatorial optimization problems [19–24]. The problem to be solved is encoded in an Ising Hamiltonian such that the solution is given by its ground state. The original algorithm is based on the quantum adiabatic time evolution from a known trivial ground state of an initial Hamiltonian to the unknown ground state of the Ising Hamiltonian [25].

However, a system in a quantum device cannot be free from environmental effects. Studying QA in a thermal environment is beneficial not only for QA devices but also to understand nonequilibrium statistical mechanics [16, 26–37].

A plausible picture of QA in the presence of a thermal environment is quasistatic and isothermal evolution, in which a system evolves maintaining a thermal equilibrium state at the temperature of its environment. This picture should be valid when the QA duration is much longer than the relaxation time of the system. Previous studies, based on a system-bath coupling realistic in the D-Wave quantum annealer [11, 15, 38, 39], have suggested that the relaxation time increases dramatically as the transverse field is reduced. Because of this increase, the quasistatic and isothermal evolution should fail near the end of annealing, and result in a final state with an effective temperature higher than that of the environment. Even though this picture has only been studied in small-sized systems, the scalings of the physical quantities expected in the thermodynamic limit have not yet been studied. In this letter, we develop a phenomenological theory and derive a novel scaling relation of the energy after QA. This scaling is valid when the temperature of the environment is sufficiently high and/or QA is sufficiently slow.

To study the QA of a system with an experimentally realistic system-bath coupling, we employ a novel numerical non-

Markovian method proposed by the present authors in Ref. [40]. This method makes use of the discrete-time path integral for a dissipative system [41] and the infinite time-evolving block decimation (iTEBD) algorithm [42], which enable the computation of the reduced density matrix (RDM) in and out of equilibrium of the translationally invariant quantum Ising chain in the thermodynamic limit. We verify the theoretical consequences on QA in a thermal environment using this method.

Model.— We consider the dissipative quantum Ising chain (DQIC) described by the Hamiltonian $H(s) = H_S(s) + H_B + H_{SB}$, where $H_S(s)$ represents the system Hamiltonian given by the quantum Ising chain,

$$H_S(s) = A(s)H_{TF} + B(s)H_I, \quad (1)$$

with $H_{TF} = -\sum_{j=1}^N \hat{\sigma}_j^x$ and $H_I = -\sum_{j=1}^{N-1} \hat{\sigma}_j^z \hat{\sigma}_{j+1}^z$. Here $\hat{\sigma}_j^x$ and $\hat{\sigma}_j^z$ denote the Pauli matrices for the site j , N is the number of sites, and s is a parameter ranging from 0 to 1. The schedule functions, $A(s)$ and $B(s)$, are assumed to be

$$A(s) = (1-s)^\alpha, \quad B(s) = s, \quad (2)$$

where an exponent $\alpha > 0$ in $A(s)$ represents how the transverse field goes to zero at the end of annealing. The bath Hamiltonian is represented by the collection of harmonic oscillators, $H_B = \sum_{j=1}^N \sum_k \omega_k \hat{b}_{j,k}^\dagger \hat{b}_{j,k}$, where $\hat{b}_{j,k}$ and $\hat{b}_{j,k}^\dagger$ are the annihilation and creation operators, respectively, of the boson for the site j and mode k with the frequency ω_k . We use the unit $\hbar = 1$ throughout this letter. As for the interaction between the system and the bath, we assume the Caldeira–Leggett model [43, 44] for dissipative superconductor flux qubits given by

$$H_{SB} = \sum_{j=1}^N \hat{\sigma}_j^z \sum_k \lambda_k \left(\hat{b}_{j,k}^\dagger + \hat{b}_{j,k} \right), \quad (3)$$

where λ_k is a coupling constant for the mode k . We assume the Ohmic spectral density for the bath modes,

$$J(\omega) = \sum_k \lambda_k^2 \delta(\omega - \omega_k) = \frac{\eta}{2} \omega e^{-\omega/\omega_c}, \quad (4)$$

where η is the dimensionless coupling constant and ω_c is the cut-off frequency of the spectrum of the bath, which is chosen to be larger than the bath temperature. When we mention QA, we consider the time evolution with time t from $t = 0$ to t_a by the Hamiltonian $H(t/t_a)$.

The dynamics of the spin system is specified by the RDM defined by tracing out the bosonic degrees of freedom from the density matrix $\rho(t)$ of the full system,

$$\rho_S(t) \equiv \text{Tr}_B \rho(t) = \text{Tr}_B [\mathcal{U}(t)\rho(0)\mathcal{U}^\dagger(t)], \quad (5)$$

where $\text{Tr}_{B(S)}$ stands for the trace with respect to the boson (spin) degrees of freedom, $\mathcal{U}(t)$ is the time evolution operator of the full system and $\rho(0)$ is an initial density matrix. We assume that $\rho(0)$ is the direct product of the ground state of $H_S(0)$ denoted by $|\psi_0(0)\rangle$ and the thermal equilibrium state of H_B at the temperature T_B : $\rho(0) = |\psi_0(0)\rangle\langle\psi_0(0)| \otimes e^{-H_B/T_B}/Z_B$, where Z_B is the partition function of H_B . We refer to T_B as the bath temperature. We chose the Boltzmann constant k_B to be the temperature unit throughout this letter.

The spin state in the instantaneous thermal equilibrium at s and temperature T is given by

$$\rho_S^{\text{eq}}(s, T) \equiv \text{Tr}_B [e^{-H(s)/T}]/Z(s, T), \quad (6)$$

where $Z(s, T)$ is the partition function of the full system. We define the Gibbs state of H_I as

$$\rho_I^{\text{eq}}(T) \equiv e^{-H_I/T}/\text{Tr}_S [e^{-H_I/T}]. \quad (7)$$

Note that $\rho_S^{\text{eq}}(s, T)$ at $s = 1$ reduces to $\rho_I^{\text{eq}}(T)$ because $H_S(1)$ commutes with H_{SB} and $\text{Tr}_B e^{-(H_S+H_{SB})/T}$ is independent of σ_j^z , which is shown by introducing new boson operators $\tilde{b}_{j,k} \equiv b_{j,k} + \lambda_k \sigma_j^z / \omega_k$ for all j and k .

Non-Markovian iTEBD.— We focus on a time-dependent state and outline the numerical method [40] used to compute Eq. (5). The application to the equilibrium RDM in Eq. (6) is straightforward.

Let us apply the Trotter decomposition [45, 46] with a step size $\Delta t = t/M$ and the Trotter number M to $\mathcal{U}(t)$ in Eq. (5), and perform the Gaussian integral with respect to the bosonic degrees of freedom. The resulting discrete-time path integral formula of the RDM is given by

$$\langle \sigma^{(M)} | \rho_S(t) | \sigma^{(M+1)} \rangle = \sum_{\{\sigma_j^{(l)} = \pm 1\}_{l \neq M, M+1}} e^{iS_0 + \mathcal{S}_{\text{infl}}}, \quad (8)$$

where $\sigma_j^{(l)}$ is the Ising-spin variable at the site j and the time t_l is defined as

$$t_l = \begin{cases} l\Delta t & (0 \leq l \leq M) \\ (2M+1-l)\Delta t & (M+1 \leq l \leq 2M+1), \end{cases} \quad (9)$$

and $|\sigma^{(l)}\rangle$ denotes the eigenstate of σ_j^z with the eigenvalue $\sigma_j^{(l)}$ [43, 47]. S_0 denotes the action of the isolated spin system.

The influence action $\mathcal{S}_{\text{infl}}$ induced by coupling to the bath is given by

$$\mathcal{S}_{\text{infl}} = \sum_{j=1}^N \sum_{l>m}^{|t_l - t_m| < \tau_c} \kappa_{l,m} \sigma_j^{(l)} \sigma_j^{(m)}, \quad (10)$$

where

$$\kappa_{l,m} = \Delta t^2 \int_0^\infty d\omega J(\omega) \frac{\cosh[\omega/(2T_B) - i\omega(t_l - t_m)]}{\sinh[\omega/(2T_B)]}. \quad (11)$$

Note that τ_c in Eq. (10) is the memory time cut-off introduced to reduce the computational cost.

The key idea of our method is to represent the part of $\exp \mathcal{S}_{\text{infl}}$ associated with a site j in terms of a matrix product state (MPS) as follows:

$$\begin{aligned} & \exp \left(\sum_{l>m}^{|t_l - t_m| < \tau_c} \kappa_{l,m} \sigma_j^{(l)} \sigma_j^{(m)} \right) \\ & \approx \sum_{\{\mu_{j,l}\}}^{\chi_t} \phi_{\mu_{j,0}}^{(j,0)S_j^{(0)}} \phi_{\mu_{j,0}, \mu_{j,1}}^{(j,1)S_j^{(1)}} \phi_{\mu_{j,1}, \mu_{j,2}}^{(j,2)S_j^{(2)}} \cdots \phi_{\mu_{j,M-1}}^{(j,M)S_j^{(M)}}, \end{aligned} \quad (12)$$

where $S_j^{(l)} \equiv (\sigma_j^{(l)}, \sigma_j^{(2M+1-l)})$ denotes the composite variable and χ_t is the bond dimension which controls the precision of the approximation in this MPS representation. Using Eq. (12) in Eq. (8), we obtain a tensor network representation for the RDM:

$$\begin{aligned} & \langle \sigma^{(M)} | \rho_S(t) | \sigma^{(M+1)} \rangle \approx \\ & \sum_{\{S_j^{(l)}, \mu_{j,l}\}_{l \neq M}} e^{iS_0} \prod_{j=1}^N \phi_{\mu_{j,0}}^{(j,0)S_j^{(0)}} \left[\prod_{l=1}^{M-1} \phi_{\mu_{j,l-1}, \mu_{j,l}}^{(j,l)S_j^{(l)}} \right] \phi_{\mu_{j,M-1}}^{(j,M)S_j^{(M)}}. \end{aligned} \quad (13)$$

Having obtained this tensor network representation, the iTEBD algorithm can be applied to implement the sum with respect to $\{S_j^{(l)}, \mu_{j,l}\}_{l \neq M}$ and compute local quantities, taking $N \rightarrow \infty$ and using the translational invariance in space [42].

Phenomenological theory.— Let us assume a finite bath temperature $T_B > 0$. In the limiting case of $t_a \rightarrow \infty$, QA in this thermal environment leads to the quasistatic and isothermal process. Accordingly, the final state of the spin system is described by $\rho_S^{\text{eq}}(1, T_B) = \rho_I^{\text{eq}}(T_B)$. When t_a is finite, the spin system approximately maintains thermal equilibrium as long as the relaxation time of the spin system is shorter than the annealing time scale. However, as we elaborate below, the relaxation time grows infinitely with $s \rightarrow 1$. Therefore, the quasistatic and isothermal evolution must fail before QA ends, and the spin state is expected to be frozen at a time $t^* = s^* t_a$.

We refer to t^* or s^* as the freezing time. To develop a scaling theory for the freezing time, we employ the quasistatic-freezing approximation as follows. The quasistatic-freezing approximation assumes that the spin state is frozen when the changing rate with t of the instantaneous relaxation time of

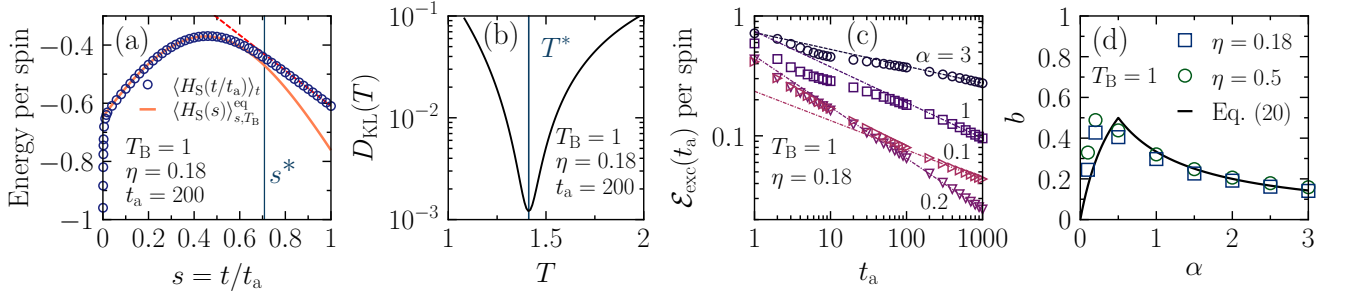


FIG. 1. (a) Energy expectation values, $\langle H_S(t/t_a) \rangle_t$ and $\langle H_S(s) \rangle_{s, T_B}^{\text{eq}}$, per spin of the time-dependent state $\rho_S(t)$ and the instantaneous thermal equilibrium state $\rho_S^{\text{eq}}(s, T_B)$, respectively, as functions of the rescaled time s for $t_a = 200$ and $\eta = 0.18$ at $T_B = 1$. We fixed $\alpha = 1$. The dashed line and the solid vertical line indicate $\frac{1}{N} \langle H_I \rangle_{t_a} t/t_a$ and $s^* \equiv T_B/T^*$, respectively, where T^* is determined by the minimization of the Kullback–Leibler (KL) divergence. (b) KL divergence $D_{\text{KL}}(T)$ between the final state after QA and the Gibbs state of H_I with temperature T . See the main text for a detailed definition. (c) Excess energy \mathcal{E}_{exc} per spin from the thermal expectation value after QA as a function of t_a for various α . Lines indicate the best power-law fits $\mathcal{E}_{\text{exc}} = at_a^{-b}$ to the data for $t_a > 100$ with the fitting parameters a and b . (d) Exponent b as a function of α . The numerical results (symbols) are compared to the theoretical prediction shown by the solid line. The parameters used in the numerical simulations are $\omega_c = 5$, $\tau_c = 10$, $\Delta t = 0.05$ and $N \rightarrow \infty$. The bond dimensions are up to 128.

the spin system exceeds unity. Writing the instantaneous relaxation time at $s = t/t_a$ as $\tau_{\text{rel}}(s)$, the freezing time is then determined by

$$\dot{\tau}_{\text{rel}}(s^*) = 1, \quad (14)$$

where the dot denotes differentiation by t . $\tau_{\text{rel}}(s)$ is now estimated from the transition rate $\gamma(s)$. Using Fermi's golden rule, the latter is given, up to an s -independent factor, as

$$\gamma_{l,m}(s) \propto \eta |\langle \psi_l(s) | \sum_i \hat{\sigma}_i^z | \psi_m(s) \rangle|^2 \quad (15)$$

where $|\psi_l(s)\rangle$ and $|\psi_m(s)\rangle$ are the l -th and m -th eigenstates of $H_S(s)$, respectively. For sufficiently large t_a , the freezing time s^* must be close to 1. Accordingly, the perturbation expansion for the eigenstates can be evoked around $s = 1$, which yields

$$\tau_{\text{rel}}(s) \approx \gamma_{l,m}(s)^{-1} \sim \eta^{-1} A(s)^{-2} \sim \eta^{-1} (1-s)^{-2\alpha}. \quad (16)$$

Using this in Eq. (14), the scaling relation of s^* is obtained as follows:

$$(1-s^*) \sim (\eta t_a)^{-1/(2\alpha+1)}. \quad (17)$$

Now, the quasistatic-freezing approximation implies that the RDM after the freezing time is approximately replaced by that of the instantaneous thermal equilibrium at $s = s^*$, namely, $\rho_S(t) \approx \rho_S^{\text{eq}}(s^*, T_B)$ for $t > s^* t_a$. Moreover, $\rho_S^{\text{eq}}(s^*, T_B)$ is approximated as $\rho_S^{\text{eq}}(s^*, T_B) = \rho_I^{\text{eq}}(T_B/s) + O(1-s^*)^\alpha$. Therefore, neglecting the $O(1-s^*)^{2\alpha}$ and $O((1-s)^\alpha(1-s^*)^\alpha)$ terms for $\alpha > \frac{1}{2}$, the energy of the spin system for $t > s^* t_a$ is estimated to be

$$\langle H_S(t/t_a) \rangle_t \approx B(t/t_a) \langle H_I \rangle_{I, T_B/s^*}^{\text{eq}}, \quad (18)$$

where $\langle \cdot \rangle_t$ and $\langle \cdot \rangle_{I, T}^{\text{eq}}$ represent the expectation values with respect to $\rho_S(t)$ and $\rho_I^{\text{eq}}(T)$, respectively. Therefore, the

energy of the spin system approaches the thermal expectation value of H_I at the temperature T_B/s^* in a linear fashion with s as $s \rightarrow 1$. For generic $\alpha > 0$, $\langle H_S(1) \rangle_{t_a} \approx \langle H_S(1) \rangle_{I, T_B}^{\text{eq}} + c(T_B)(1-s^*)^{\min\{1, 2\alpha\}}$, where $c(T)$ is a function of T which is independent of s^* . Applying Eq. (17), the excess energy of the final state is obtained as

$$\mathcal{E}_{\text{exc}} \equiv \langle H_S(1) \rangle_{t_a} - \langle H_S(1) \rangle_{I, T_B}^{\text{eq}} \sim (\eta t_a)^{-b}, \quad (19)$$

with

$$b = \min\{1, 2\alpha\}/(\alpha + 1). \quad (20)$$

Note that the excess energy decays the fastest when $\alpha = \frac{1}{2}$. Equations (19) and (20) are valid for DQIC in any dimension and any lattice.

Numerical results.— Figure 1(a) shows the energy expectation value per site of the time-dependent state during QA and that of the instantaneous thermal equilibrium as functions of the rescaled time s . After the initial relaxation, the system maintains thermal equilibrium until a certain time s^* , when the quasistatic and isothermal evolution fails and the energy deviates upwards from that of the instantaneous equilibrium state. This behavior is perfectly consistent with the quasistatic-freezing picture mentioned above. To evaluate the freezing time s^* and identify the final energy $\langle H_I \rangle_{t_a}$, we focus on the Kullback–Leibler (KL) divergence D_{KL} of the final state and the Boltzmann distribution of H_I as a measure of the distance between the two. Because this quantity is not accessible for the RDMs of the entire spin system when using our method, we instead consider the RDMs of eight spins given by $\rho_8 \equiv \text{Tr}_{\bar{8}} \rho_S(t_a)$ and $\rho_8^{\text{eq}}(T) \equiv \text{Tr}_{\bar{8}} \rho_I^{\text{eq}}(T)$ to define $D_{\text{KL}}(T) \equiv \text{Tr}_8 [\rho_8 (\log \rho_8 - \log \rho_8^{\text{eq}}(T))]$, where Tr_8 and $\text{Tr}_{\bar{8}}$ denote the trace with respect to the eight adjacent spins and the other spins, respectively. We show $D_{\text{KL}}(T)$ in Fig. 1(b). $D_{\text{KL}}(T)$ has a sharp minimum at a certain T labeled T^* . This implies that the RDM after QA is approximated by the Gibbs

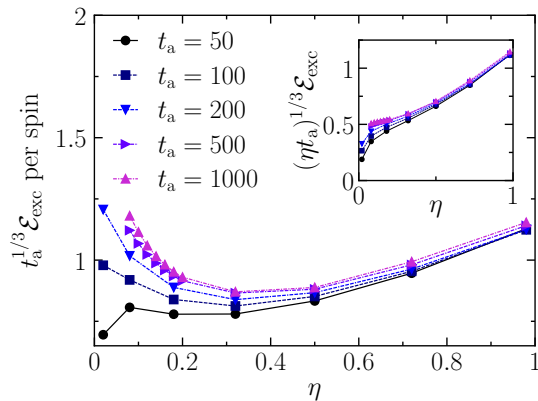


FIG. 2. Excess energy per spin after QA scaled by $t_a^{-1/3}$ as a function of η for $T_B = 1$, $\alpha = 1$, and various t_a ranging from 50 to 1000. With increasing t_a , the data collapse into a single nonmonotonic curve, which implies $\mathcal{E}_{\text{exc}} \sim t_a^{-1/3}$ for large t_a . The inset shows the data rescaled by $(\eta t_a)^{-1/3}$. The constancy of the data with large t_a near $\eta = 0$ corresponds to Eq. (19). The parameters in the numerical simulations are the same as those in Fig. 1.

state of H_I with the temperature T^* . In addition, as shown in Fig. 1(a), the curve of $\langle H_S(t/t_a) \rangle_t$ is indistinguishable from the line of $s\langle H_I \rangle_{1,T^*}$ near $s = 1$. Assuming $T^* = T/s^*$, this result implies Eq. (18) and that s^* determined by T/T^* is consistent with the freezing time when the quasistatic evolution fails (see the vertical line in Fig. 1(a)). Figure 1(c) shows the excess energy as a function of the annealing time t_a for $\eta = 0.18$ and $T_B = 1$. It can be seen that the excess energy decays as a power law for large t_a with an exponent denoted by b that depends on α . Figure 1(d) shows the α dependence of the exponent b . There is excellent agreement between the numerical results and the theoretical prediction.

Figure 2 shows the η -dependence of \mathcal{E}_{exc} scaled by $t_a^{1/3}$ for $T_B = 1$, $\alpha = 1$, and various t_a . It can be seen that \mathcal{E}_{exc} is nonmonotonic with respect to η . The decreasing behavior of \mathcal{E}_{exc} with increasing η in the weak coupling regime is consistent with Eq. (19), while its increasing behavior in the strong-coupling regime ($\eta \gtrsim 0.4$) is not described by the phenomenological theory mentioned above. This failure of the theory arises from the perturbative argument used for the relaxation time in Eq. (15). The existence of the optimal strength in the system-bath coupling to reduce \mathcal{E}_{exc} is first revealed by our numerical method based on a non-perturbative formulation. Note that the scaling of \mathcal{E}_{exc} by t_a is valid even in the strong-coupling situation.

So far, we have focused on slow QA in a thermal environment with a finite temperature and have discussed consequences of freezing near the end of annealing. Here, we comment on two situations where the dynamics is governed by a quantum phase transition at zero temperature, assuming the absence of a thermal phase transition at finite temperature. The first is a weak-coupling and short-annealing-time situation. When the system-bath coupling is sufficiently weak, i.e.

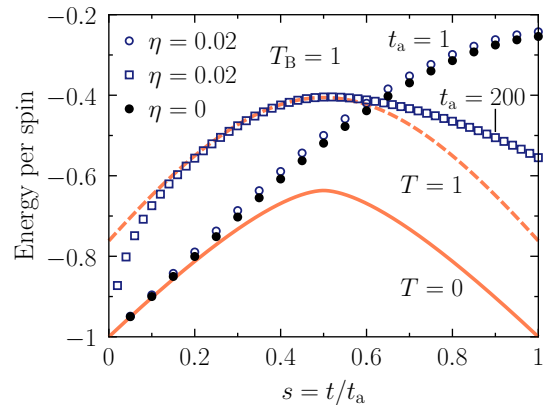


FIG. 3. Energy expectation values per spin as functions of the rescaled time s . The solid line shows the energy of the instantaneous ground state of $H_S(s)$. The filled symbols show the energy of the time-dependent state for $t_a = 1$ of the closed system ($\eta = 0$). The empty symbols denote energies of the time-dependent states of the dissipative system with $\eta = 0.02$ and $T_B = 1$ for $t_a = 1$ and $t_a = 200$. We fixed $\alpha = 1$. The parameters in the numerical simulations are the same as those in Fig. 1.

$\eta \ll 1$, QA drives the spin system in the same way as a closed system as long as t_a is not large, as demonstrated by the circles in Fig. 3. This insensitivity to the environment gives rise to the Kibble–Zurek scaling (KZS) [48–50] of the residual energy to the ground state after QA, which is a manifestation of a quantum phase transition. For larger t_a , the system is thermalized and the final state gains an excess energy as shown by the squares in Fig. 3. This crossover is accompanied by an increase in the residual energy over a certain parameter range [51]. The second is a medium-coupling and low-temperature situation, where the dynamics is governed by a quantum phase transition of the dissipative system at $T = 0$. In this case, KZS with a modified exponent [40] is observed. When the temperature is not low and/or t_a is much larger, however, the spin system is not influenced by a quantum phase transition and the quasistatic-freezing picture is valid because the time scale of QA is beyond the characteristic time in the quantum critical region [51]. A recent experimental study suggested that systems realized in the D-Wave device should be in a situation with a medium η and a low T [36]. Therefore, if one performs experiments with still longer t_a or higher T , the scaling of the excess energy given by Eqs. (19) and (20) should be observed.

Summary.— We developed a phenomenological theory for QA in a thermal environment based on the quasistatic-freezing approximation. The theoretical results were numerically confirmed using a novel non-Markovian iTEBD method. The theoretical and numerical findings presented here will be beneficial in designing and evaluating QA devices.

The authors acknowledge H. Nishimori and Y. Susa for valuable discussions, and Y. Bando, M. Ohzeki, F. J. Gómez-Ruiz, A. del Campo, and D. A. Lidar for collaboration on a

related experimental project.

* hiroki.oshiyama.e6@tohoku.ac.jp

† sei01@saitama-med.ac.jp

‡ shibata@cmtpt.phys.tohoku.ac.jp

§ Present address: Graduate School of Information Sciences, Tohoku University, Sendai 980-8578, Japan

- [1] M. W. Johnson, M. H. Amin, S. Gildert, T. Lanting, F. Hamze, N. Dickson, R. Harris, A. J. Berkley, J. Johansson, P. Bunyk, E. M. Chapple, C. Enderud, J. P. Hilton, K. Karimi, E. Ladizinsky, N. Ladizinsky, T. Oh, I. Perminov, C. Rich, M. C. Thom, E. Tolkacheva, C. J. Truncik, S. Uchaikin, J. Wang, B. Wilson, and G. Rose, *Nature* **473**, 194 (2011).
- [2] S. Boixo, T. F. Rønnow, S. V. Isakov, Z. Wang, D. Wecker, D. A. Lidar, J. M. Martinis, and M. Troyer, *Nature Physics* **10**, 218 (2014).
- [3] V. S. Denchev, S. Boixo, S. V. Isakov, N. Ding, R. Babbush, V. Smelyanskiy, J. Martinis, and H. Neven, *Phys. Rev. X* **6**, 031015 (2016).
- [4] T. Albash and D. A. Lidar, *Phys. Rev. X* **8**, 031016 (2018).
- [5] A. D. King, J. Carrasquilla, J. Raymond, I. Ozfidan, E. Andriyash, A. Berkley, M. Reis, T. Lanting, R. Harris, F. Altomare, K. Boothby, P. I. Bunyk, C. Enderud, A. Fréchet, E. Hoskinson, N. Ladizinsky, T. Oh, G. Poulin-Lamarre, C. Rich, Y. Sato, A. Y. Smirnov, L. J. Swenson, M. H. Volkman, J. Whittaker, J. Yao, E. Ladizinsky, M. W. Johnson, J. Hilton, and M. H. Amin, *Nature* **560**, 456 (2018).
- [6] R. Harris, Y. Sato, A. J. Berkley, M. Reis, F. Altomare, M. H. Amin, K. Boothby, P. Bunyk, C. Deng, C. Enderud, S. Huang, E. Hoskinson, M. W. Johnson, E. Ladizinsky, N. Ladizinsky, T. Lanting, R. Li, T. Medina, R. Molavi, R. Neufeld, T. Oh, I. Pavlov, I. Perminov, G. Poulin-Lamarre, C. Rich, A. Smirnov, L. Swenson, N. Tsai, M. Volkman, J. Whittaker, and J. Yao, *Science* **361**, 162 (2018).
- [7] A. D. King, J. Raymond, T. Lanting, S. V. Isakov, M. Mohseni, G. Poulin-Lamarre, S. Ejtemaei, W. Bernoudy, I. Ozfidan, A. Y. Smirnov, M. Reis, F. Altomare, M. Babcock, C. Baron, A. J. Berkley, K. Boothby, P. I. Bunyk, H. Christiani, C. Enderud, B. Evert, R. Harris, E. Hoskinson, S. Huang, K. Jooya, A. Khodabandelou, N. Ladizinsky, R. Li, P. A. Lott, A. J. R. MacDonald, D. Marsden, G. Marsden, T. Medina, R. Molavi, R. Neufeld, M. Norouzpour, T. Oh, I. Pavlov, I. Perminov, T. Prescott, C. Rich, Y. Sato, B. Sheldan, G. Sterling, L. J. Swenson, N. Tsai, M. H. Volkman, J. D. Whittaker, W. Wilkinson, J. Yao, H. Neven, J. P. Hilton, E. Ladizinsky, M. W. Johnson, and M. H. Amin, “Scaling advantage in quantum simulation of geometrically frustrated magnets,” (2019), arXiv:1911.03446 [quant-ph].
- [8] H. Ushijima-Mwesigwa, C. F. A. Negre, and S. M. Mniszewski, in *Proceedings of the Second International Workshop on Post Moores Era Supercomputing, PMES’17* (Association for Computing Machinery, New York, NY, USA, 2017) pp. 22–29, event-place: Denver, CO, USA.
- [9] A. Teplukhin, B. K. Kendrick, S. Tretiak, and P. A. Dub, *Scientific Reports* **10**, 20753 (2020).
- [10] S. Boixo, T. Albash, F. M. Spedalieri, N. Chancellor, and D. A. Lidar, *Nature Communications* **4**, 2067 (2013).
- [11] J. Marshall, E. G. Rieffel, and I. Hen, *Phys. Rev. Applied* **8**, 064025 (2017).
- [12] M. S. Sarandy and D. A. Lidar, *Phys. Rev. Lett.* **95**, 250503 (2005).
- [13] M. H. S. Amin, P. J. Love, and C. J. S. Truncik, *Phys. Rev. Lett.* **100**, 060503 (2008).
- [14] N. G. Dickson, M. W. Johnson, M. H. Amin, R. Harris, F. Altomare, A. J. Berkley, P. Bunyk, J. Cai, E. M. Chapple, P. Chavez, F. Cioata, T. Cirip, P. deBuen, M. Drew-Brook, C. Enderud, S. Gildert, F. Hamze, J. P. Hilton, E. Hoskinson, K. Karimi, E. Ladizinsky, N. Ladizinsky, T. Lanting, T. Mahon, R. Neufeld, T. Oh, I. Perminov, C. Petroff, A. Przybysz, C. Rich, P. Spear, A. Teaciuc, M. C. Thom, E. Tolkacheva, S. Uchaikin, J. Wang, A. B. Wilson, Z. Merali, and G. Rose, *Nature Communications* **4**, 1903 (2013).
- [15] M. H. Amin, *Phys. Rev. A* **92**, 052323 (2015).
- [16] L. Arceci, S. Barbarino, R. Fazio, and G. E. Santoro, *Phys. Rev. B* **96**, 054301 (2017).
- [17] V. N. Smelyanskiy, D. Venturelli, A. Perdomo-Ortiz, S. Knys, and M. I. Dykman, *Phys. Rev. Lett.* **118**, 066802 (2017).
- [18] A. Y. Smirnov and M. H. Amin, *New Journal of Physics* **20**, 103037 (2018).
- [19] T. Kadowaki and H. Nishimori, *Phys. Rev. E* **58**, 5355 (1998).
- [20] A. Finnila, M. Gomez, C. Sebenik, C. Stenson, and J. Doll, *Chemical Physics Letters* **219**, 343 (1994).
- [21] A. Das and B. K. Chakrabarti, eds., *Quantum annealing and related optimization methods* (Springer, Berlin, Heidelberg, 2005) lecture Notes in Physics, Vol. 679.
- [22] A. Das and B. K. Chakrabarti, *Rev. Mod. Phys.* **80**, 1061 (2008).
- [23] T. Albash and D. A. Lidar, *Rev. Mod. Phys.* **90**, 015002 (2018).
- [24] P. Hauke, H. G. Katzgraber, W. Lechner, H. Nishimori, and W. D. Oliver, *Reports on Progress in Physics* **83**, 054401 (2020).
- [25] E. Farhi, J. Goldstone, S. Gutmann, J. Lapan, A. Lundgren, and D. Preda, *Science* **292**, 472 (2001).
- [26] D. Patanè, A. Silva, L. Amico, R. Fazio, and G. E. Santoro, *Phys. Rev. Lett.* **101**, 175701 (2008).
- [27] D. Patanè, L. Amico, A. Silva, R. Fazio, and G. E. Santoro, *Phys. Rev. B* **80**, 024302 (2009).
- [28] S. Yin, P. Mai, and F. Zhong, *Phys. Rev. B* **89**, 094108 (2014).
- [29] M.-J. Hwang, R. Puebla, and M. B. Plenio, *Phys. Rev. Lett.* **115**, 180404 (2015).
- [30] P. Nalbach, S. Vishveshwara, and A. A. Clerk, *Phys. Rev. B* **92**, 014306 (2015).
- [31] A. Dutta, A. Rahmani, and A. del Campo, *Phys. Rev. Lett.* **117**, 080402 (2016).
- [32] M. Keck, S. Montangero, G. E. Santoro, R. Fazio, and D. Rossini, *New Journal of Physics* **19**, 113029 (2017).
- [33] P. Weinberg, M. Tylutki, J. M. Rönkkö, J. Westerholm, J. A. Åström, P. Manninen, P. Törmä, and A. W. Sandvik, *Phys. Rev. Lett.* **124**, 090502 (2020).
- [34] R. Puebla, A. Smirne, S. F. Huelga, and M. B. Plenio, *Phys. Rev. Lett.* **124**, 230602 (2020).
- [35] D. Rossini and E. Vicari, *Phys. Rev. Research* **2**, 023211 (2020).
- [36] Y. Bando, Y. Susa, H. Oshiyama, N. Shibata, M. Ohzeki, F. J. Gómez-Ruiz, D. A. Lidar, S. Suzuki, A. del Campo, and H. Nishimori, *Phys. Rev. Research* **2**, 033369 (2020).
- [37] S. Bandyopadhyay, S. Bhattacharjee, and A. Dutta, *Phys. Rev. B* **101**, 104307 (2020).
- [38] T. Albash, S. Boixo, D. A. Lidar, and P. Zanardi, *New Journal of Physics* **14**, 123016 (2012).
- [39] J. Marshall, D. Venturelli, I. Hen, and E. G. Rieffel, *Phys. Rev. Applied* **11**, 044083 (2019).
- [40] H. Oshiyama, N. Shibata, and S. Suzuki, *J. Phys. Soc. Japan* **89**, 1 (2020).
- [41] N. Makri, *Chemical Physics Letters* **193**, 435 (1992).
- [42] R. Orús and G. Vidal, *Phys. Rev. B* **78**, 155117 (2008).

- [43] A. O. Caldeira and A. J. Leggett, *Ann. Phys. (N. Y.)* **149**, 374 (1983).
- [44] A. J. Leggett, S. Chakravarty, A. T. Dorsey, M. P. A. Fisher, A. Garg, and W. Zwerger, *Rev. Mod. Phys.* **59**, 1 (1987).
- [45] H. F. Trotter, *Proceedings of the American Mathematical Society* **10**, 545 (1959).
- [46] M. Suzuki, *Progress of Theoretical Physics* **56**, 1454 (1976).
- [47] D. E. Makarov and N. Makri, *Chemical Physics Letters* **221**, 482 (1994).
- [48] T. W. B. Kibble, *Journal of Physics A: Mathematical and General* **9**, 1387 (1976).
- [49] W. H. Zurek, *Nature* **317**, 505 (1985).
- [50] J. Dziarmaga, *Phys. Rev. Lett.* **95**, 245701 (2005).
- [51] See Supplementary Materials.

Supplementary Materials: Classical simulation and theory of quantum annealing in a thermal environment

Hiroki Oshiyama,¹ Sei Suzuki,² and Naokazu Shibata¹

¹*Department of Physics, Tohoku University, Sendai 980-8578, Japan*

²*Department of Liberal Arts, Saitama Medical University, Moroyama, Saitama 350-0495, Japan*

In this Supplementary Materials, we supplement numerical results on the residual energy to the ground state after QA, which is defined by $\mathcal{E}_{\text{res}}(t_a) \equiv \langle H_S(1) \rangle_{t_a} - E_g(1)$ where the ground energy $E_g(1)$ of $H_S(1)$ is given by $E_g(1) = -1$.

At first, we briefly review the Kibble-Zurek scaling (KZS) of the residual energy in a closed system. When $\eta = 0$, the spin system encounters a quantum phase transition during QA with the time-dependent Hamiltonian $H_S(t)$ changing from H_{TF} to H_{I} . The system loses adiabaticity near a quantum critical point and thereby ends up with a residual energy and topological defects. The residual energy is smaller for slower QA, i.e., larger t_a . This mechanism for the residual energy due to time evolution across a continuous phase transition is called as the Kibble-Zurek mechanism (KZM) [? ?]. The scaling of the residual energy with respect to t_a is universal and given by $E_{\text{res}} \sim t_a^{-d\nu/(n\nu+1)}$ [? ?], where ν and z are the correlation-length and the dynamical critical exponents of the associated quantum critical point. This scaling of the residual energy is the KZS. In case of the transverse Ising chain, one has $\nu = z = 1$ and hence KZS leads to $E_{\text{res}} \sim t_a^{-1/2}$ [?].

Before proceeding to numerical results, we comment on KZS in the dissipative transverse Ising chain. Consider the case with $\eta > 0$ and $T = 0$. This dissipative spin system also involves a quantum phase transition. The quantum critical point forms a quantum critical line $s_c(\eta)$ in the $s - \eta$ plane. An earlier study using the quantum Monte-Carlo simulation have estimated critical exponents on this critical line as $\nu \approx 0.64$ and $z \approx 2.0$ for $\eta > 0$ [?]. These exponents suggest a modification of the KZS exponent b of $E_{\text{res}} \sim t_a^{-b}$ as $b_{\text{QMC}} \approx 0.28$ from $1/2$ of the closed system. The present authors have studied KZS of the same model by means of iTEBD in the previous work [?]. The results imply that the exponent of KZS decreases gradually from 0.5 to 0.25 with increasing η from 0 to 0.7. The qualitative tendency that the exponent declines in the presence of the environment is shared by the theoretical prediction with quantum Monte-Carlo data and numerical experiments. The quantitative inconsistency is attributed to the smallness of t_a in numerical experiments.

We now move on to numerical results for finite temperatures. Figure S1(a) shows results for $\eta = 0.02$ as a weak coupling situation. When the temperature is sufficiently low, the residual energy decreases monotonically with t_a . We expect that it should converge to the thermal expectation value, $\langle H_S(1) \rangle_{I, T_B}^{\text{eq}} + 1$, for $t_a \rightarrow \infty$. For higher T_B , the residual energy varies nonmonotonically with t_a . This nonmonotonic curve can be divided in three regions: (i) the KZS for sufficiently small t_a where E_{res} decays following the power law as that of the closed system, (ii) the anti-KZS for the middle range of t_a where E_{res} deviates from the power law and increases with t_a , and (iii) the quasistatic-freezing region for sufficiently large t_a where E_{res} decreases toward $\langle H_S(1) \rangle_{I, T_B}^{\text{eq}} + 1$. Note that the excess energy, defined by $\mathcal{E}_{\text{exc}} \equiv \langle H_S(1) \rangle_{t_a} - \langle H_S(1) \rangle_{I, T_B}^{\text{eq}}$ follows Eq. (19) in (iii) as we mentioned in the main text. This nonmonotonic anti-KZS behavior of the residual energy has been discussed in literatures [? ?]. It arises as a consequence of a large KZS region such that the residual energy at the end of the KZS region is below the thermal expectation value.

We next focus on $\eta = 0.18$ as a medium coupling situation. Figure S2 compares the energy of a time-dependent state driven by QA with that of the instantaneous equilibrium state at $T = 0$. The spin system equilibrates with the bath in an early time of annealing, keeps equilibrium approximately for a while, and then drop out of equilibrium. The result for $\eta = 0.18$ is in contrast to the one for $\eta = 0.02$ where the energy of the time-dependent state is mostly indistinguishable from that in a closed system. The upward deviation of the curve of the time-dependent state at $T = 0$ from that of the equilibrium state comes from KZM, namely, the growth of the relaxation time near a quantum critical point and the failure of a quasistatic evolution. In Fig. S3, the residual energy at $T_B = 0$ is observed to decay, following a power law with the exponent $b \approx 0.47$. As mentioned above, although this exponent is larger than $b_{\text{QMC}} \approx 0.28$ predicted from the quantum Monte-Carlo simulation, a power law confirms KZS of the residual energy in a dissipative system. Raising temperature of the bath in Fig. S3, one finds that the range of t_a for KZS shrinks and eventually vanishes. The anti-KZS is not observed here. These results are in sharp contrast to the results for the weak coupling. At finite temperatures, QA does not cross a quantum critical point. The separation from a quantum critical point is larger and the relaxation time is shorter for higher temperature. When the relaxation time maximized near a quantum critical point at finite temperature is shorter than the time scale of QA, KZM does not work and a quasistatic evolution survives until freezing near the end of QA. This is why KZS disappears for higher temperatures. The absence of the anti-KZS is because the residual energy does not drop enough with KZS.

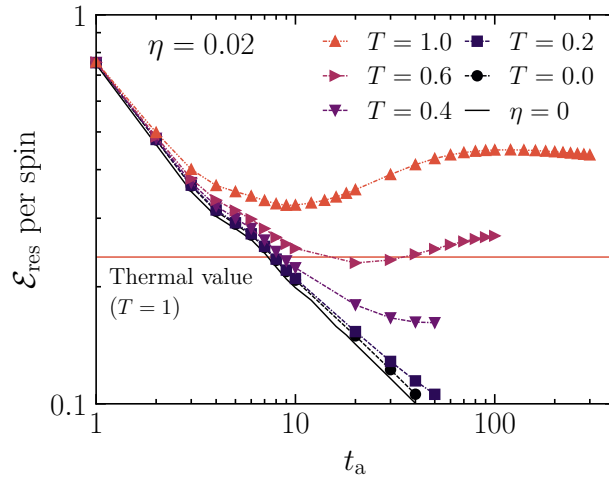


FIG. S1. Residual energy after QA as a function of annealing time t_a for a weak coupling with $\eta = 0.02$ and various temperatures. The result of the closed system is shown by the solid line for comparison. The horizontal line indicates the thermal expectation value at $T = 1$.

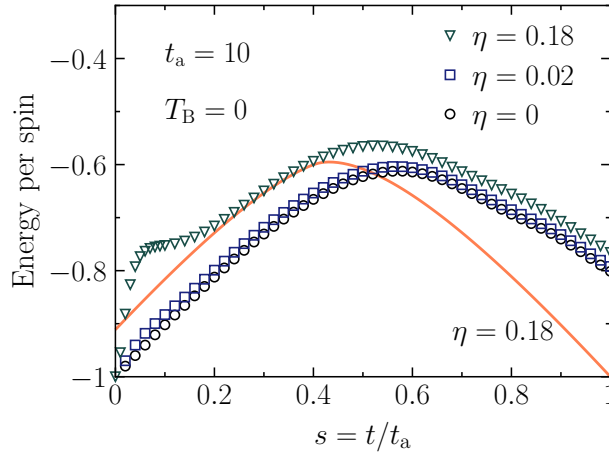


FIG. S2. Energies per spin as function of the rescaled time s of time-dependent states with $t_a = 10$ at $T_B = 0$ and of equilibrium states at $T = 0$. Squares and triangles represent results of time-dependent states for $\eta = 0.18$ and $\eta = 0.02$, respectively, while circles are for the closed system. The solid and dashed lines show the instantaneous energies per spin of the equilibrium states of the closed system at $T = 0$ and the dissipative system at $T = 0$ with $\eta = 0.18$.

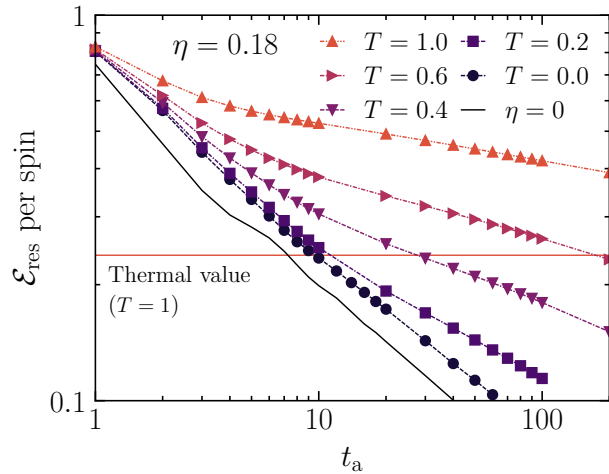


FIG. S3. Residual energy after QA as a function of annealing time t_a for a medium coupling with $\eta = 0.18$ and various temperatures. The result of the closed system is shown by the solid line for comparison. The horizontal line indicates the thermal expectation value at $T = 1$.